
**THEORETICAL AND MATHEMATICAL
PHYSICS**

Theoretical Cross-Section Calculations for the (α, n) and $(\alpha, 2n)$ Reactions on ^{46}Ti , ^{50}Cr , ^{54}Fe , and ^{93}Nb Isotopes

Mert Şekerçi*

*Süleyman Demirel University, Faculty of Arts and Sciences, Department of Physics,
Isparta, 32260 Turkey*

Received December 9, 2019; revised December 27, 2019; accepted January 9, 2020

Abstract—The employment of the fusion mechanism for the energy production is a promising solution to the continuously growing global energy demand. The correct material selection for this cutting edge technology is just as important as the efforts to understand the related nuclear reaction mechanisms. A value which is relevant to nuclear reactions and is of considerable importance is the cross-section of the reaction. Among many parameters, which affect the theoretical calculations of this quantity, level density models and alpha optical model potentials have played an important role, due to their direct effects on the calculations. By considering the importance of the materials used in the fusion technology and the aforementioned parameters, the aim of this work is to study the effects of level density models, alpha optical model potentials and their combinational usage in the cross-section theoretical calculations on the alpha particle induced reactions for ^{46}Ti , ^{50}Cr , ^{54}Fe and ^{93}Nb isotopes. The examined reaction routes are limited to the alpha particle induced single and double neutron emitting reactions. All calculations were performed by using the 1.9 version of the TALYS code, in which six level density models and eight alpha optical model potentials are available. The results of the present work are compared with the existing literature data, taken from the Experimental Nuclear Reaction Database (EXFOR) library, by performing a mean weighted deviation analysis calculation. The more consistent results in comparison with the experimental data were obtained with the combinational use of the models.

Keywords: cross-section, nuclear reaction, Experimental Nuclear Reaction Database.

DOI: 10.3103/S0027134920020095

1. INTRODUCTION

Recent research and report studies have shown that global demand for energy has increased rapidly over the last few decades and the expectation for the forthcoming years will be the continuation of this trend [1]. A possible solution to this great amount of energy request can be shown as the adaptation of the nuclear fusion mechanism for the energy production, which is accompanied by many attractive features, such as the possibility of large scale power generation with fewer resource, immense use, being free from emission of greenhouse gases, nonexistence of diverse wastes and less chance of severe accident [2, 3]. Some, among the many studies carried out to benefit from the fusion mechanism are related to the material development and to the study of the nuclear reaction mechanisms. The use of theoretical studies in cases where experimental studies cannot be performed to understand the nuclear reaction mechanisms is accepted in the literature [4–8].

There are some nuclear reaction models, such as two component exciton and Hauser–Feshbach models, developed to explain different reaction mechanisms, such as direct, pre-equilibrium and compound reaction mechanisms, and these models contain numerous parameters. Studies have been conducted to investigate the effects of theoretical nuclear reaction model parameters on various important variables which could provide a foresight to the researchers about the investigated reaction, such as the cross-section value that can be simply defined as the probability of a reaction’s occurrence [9–14]. In the process of understanding the nuclear excited states, a global description of the level density function played a highly important role. The level gaps in the discrete levels of an excited nucleus become so narrow with the increase of excitation energy, which makes it experimentally impossible to perform a definition for each excited level. In accordance to that, the use and assessment of the nuclear level density, which simply could be defined as the excited levels around an excitation energy, are necessary for the theoretical cross-

*E-mail: mertsekerci@sdu.edu.tr

section calculations [15, 16]. Therefore, level density models are crucial for the cross-section calculations and there are many studies in the literature performed to investigate their various effects on the theoretical calculations [17–22]. Another parameter, whose effects on the theoretical cross-section calculations are examined within this study, is the alpha optical model potential, which is at least as important as the level density models. The optical name was used for this concept because it was constructed and developed with an approach similar to the classical scattering of light waves. These potentials are crucial for the specification of the reaction cross-section dispersal, such as compound and pre-equilibrium, over all probable and opened reaction channels [23]. By considering the undeniable importance of these parameters on the theoretical cross-section calculations, the objective of this study is appointed as the investigation of individual and combinational use of two important models, which are the level density models and the alpha optical model potentials, for (α, n) and $(\alpha, 2n)$ reaction channels on the ^{46}Ti , ^{50}Cr , ^{54}Fe and ^{93}Nb isotopes where the elemental forms of these isotopes are used in the fusion technology.

Cross-section calculations for each investigated reaction channel were performed by employing the TALYS 1.9 code [24]. There are six level density models and eight alpha optical model potentials that can be used in the TALYS code. First, all the available level density models were employed one by one while the alpha optical model potential was assigned as the TALYS default model, which is Normal Alpha Potential. Then, similarly, all the available optical model potentials for alpha particles were employed one by one while the level density model was assigned as the TALYS default model, which is Constant Temperature + Fermi Gas Model. The results of the cross-section calculations were compared with the experimental data adopted from the Experimental Nuclear Reaction Data (EXFOR) library [25] by using a mean weighted deviation analysis [26] to determine the most consistent level density and alpha optical model potential. Then, further calculations were carried out using the level density and alpha optical potential models, which were determined as the most consistent with the experimental data. The combinational use of the level density models and alpha optical model potentials provided more consistent results in comparison with the experimental data in all reaction channels.

2. THEORETICAL CROSS-SECTION CALCULATION MODELS

The cross-section calculations performed within the scope of this study were all done by employing

the TALYS 1.9 code. TALYS is an open source multi-purpose nuclear reaction analyze code which can examine the various results and outcomes of a specific reaction in addition to the effects of different parameters on that reaction. There exist six level density models and eight alpha optical model potentials implemented in the TALYS code.

In the framework of the presented study, three phenomenological and three microscopic level density models were employed. The former models are the Constant Temperature + Fermi Gas Model (CT + FGM) [27, 28], the Back Shifted Fermi Gas Model (BSFGM) [29, 30] and the Generalised Superfluid Model (GSM) [31, 32], while the latter ones are the Skyrme Force-Goriely (SFG) [33], the Skyrme Force-Hilaire (SFH) [34] and the Gogny Force dependent (GFD) [35] model. The default level density model assigned by the TALYS is the CT + FGM, which is derived from the Fermi Gas Model (FGM) [36] like all other phenomenological models. In FGM, it is accepted that the nucleons hold the lowest possible energy levels and fill the uppers with an excitation. This assumption is improved by adopting a constant temperature approach with CT + FGM. The second model, the BSFGM, was developed by including an adjustable parameter to shift the excitation energy, while the last phenomenological model, GSM, was defined by a phase transition between the lower energies around the superfluid behavior and the higher energies characterized by FGM. Besides the phenomenological models, microscopic ones were also employed. Two of them, SFG and SFH, were developed by using the contributions of Skyrme force from the tabulated data sets of Goriely and Hilaire. On the other hand the GFD was developed by using the Gogny force from the Hilaire's combinatorial tables via temperature dependent Hartree-Fock-Bogolyubov (HFB) calculations.

Concerning the alpha optical model potential, TALYS has a default one, like it has a default level density model which is known as Normal Alpha Potential and developed by using Watanabe folding approach with Koning-Delaroche nucleon potentials [37]. Another option is the optical model parameters for alphas introduced by McFadden and Satchler [38], which was developed by examining the elastic scattering of the alpha particles. In addition, three more alpha optical model potentials are available in the TALYS code from the study of Demetriou et al. [39], in which two tables for the parameters of the imaginary potential are introduced in addition to a dispersive model. Furthermore a highly important study of Avrigeanu et al. [40], in which the existing alpha particle induced reaction channels were examined for the nuclei of mass number $121 \leq A \leq 197$

Table 1. Mean weighted deviation analysis results of employed six level density model calculations for each reaction route with respect to the experimental data taken from EXFOR

Reaction Route	TALYS 1.9 CT + FGM	TALYS 1.9 BSFGM	TALYS 1.9 GSM	TALYS 1.9 SFG	TALYS 1.9 SFH	TALYS 1.9 GFD
$^{46}\text{Ti}(\alpha, n)^{49}\text{Cr}$	3.19815	3.17653	2.89516	4.03325	3.16435	3.24873
$^{46}\text{Ti}(\alpha, 2n)^{48}\text{Cr}$	4.75317	3.12142	3.18826	6.87732	4.38645	5.41150
$^{50}\text{Cr}(\alpha, n)^{53}\text{Fe}$	59.21586	45.64500	52.79202	72.49834	52.89675	44.42287
$^{50}\text{Cr}(\alpha, 2n)^{52}\text{Fe}$	5.25741	4.59839	4.41138	5.91315	4.98953	4.59652
$^{54}\text{Fe}(\alpha, n)^{57}\text{Ni}$	5.06814	5.07165	4.90037	4.98487	5.10341	5.56642
$^{54}\text{Fe}(\alpha, 2n)^{56}\text{Ni}$	4.52688	3.44726	5.69600	6.99270	8.24977	14.20558
$^{93}\text{Nb}(\alpha, n)^{96}\text{Tc}$	16.56623	17.98068	19.19671	20.71274	19.89706	33.54877
$^{93}\text{Nb}(\alpha, 2n)^{95}\text{Tc}$	23.43376	21.36944	26.70250	24.90955	29.46975	32.05715

to provide a better understanding of the interactions between the nucleus and the incident particle below Coulomb barrier was tested. Nolte et al. [41], was tested the outcomes of both elastic and inelastic scattering data in their study and a set of parameters from this study were used in the TALYS as a different alpha optical model potential. Beside these models and previously mentioned models developed from the study of Avrigeanu et al. [40], the last option of TALYS was adopted from the study of Avrigeanu et al. [42].

In order to determine the most consistent level density models and alpha optical model potentials for each investigated reaction channel, the results obtained from the cross-section calculations using the aforementioned models were compared with the available experimental data using the mean weighted deviation analysis shown by the following equation [26].

$$F = \left[\frac{1}{N} \sum_{i=1}^N \left[\left(\sigma_i^{calc} - \sigma_i^{expr} \right) / \Delta \sigma_i^{expr} \right]^2 \right]^{1/2} \quad (1)$$

In Eq. (1), σ_i^{calc} is the calculated cross-section, while σ_i^{expr} and $\Delta \sigma_i^{expr}$ are the experimental cross-section and its uncertainty, respectively, for the amount of N data. The mean weighted deviation result, which is represented with F , is a measure of the consistency between the theoretical calculations and the experimental data. A better consensus is provided with the lower F values [26].

3. RESULTS AND DISCUSSION

In accordance with the aim of this study, individual level density model and alpha optical model potentials

were employed for the reaction cross-section calculations. Also, their combinational usages were tested by employing the determined most consistent level density model-alpha optical model potential pair with respect to the experimental data. Calculations were done for the $^{46}\text{Ti}(\alpha, n)^{49}\text{Cr}$, $^{46}\text{Ti}(\alpha, 2n)^{48}\text{Cr}$, $^{50}\text{Cr}(\alpha, n)^{53}\text{Fe}$, $^{50}\text{Cr}(\alpha, 2n)^{52}\text{Fe}$, $^{54}\text{Fe}(\alpha, n)^{57}\text{Ni}$, $^{54}\text{Fe}(\alpha, 2n)^{56}\text{Ni}$, $^{93}\text{Nb}(\alpha, n)^{96}\text{Tc}$ and $^{93}\text{Nb}(\alpha, 2n)^{95}\text{Tc}$ reaction channels. Obtained results were graphically compared in the Figs. 1–8. In addition, Tables 1–4 were given to represent the results of the mean weighted deviation analyses.

The cross-section theoretical calculations results for the $^{46}\text{Ti}(\alpha, n)^{49}\text{Cr}$ and $^{46}\text{Ti}(\alpha, 2n)^{48}\text{Cr}$ reaction channels are presented in Figs. 1 and 2, respectively, along with the existing experimental data in the EXFOR library. Concerning the $^{46}\text{Ti}(\alpha, n)^{49}\text{Cr}$ reaction, the most consistent level density model is determined to be the GSM and be as BSFGM for the $^{46}\text{Ti}(\alpha, 2n)^{48}\text{Cr}$ reaction. Regarding the alpha optical model parameters, the most consistent results were obtained for the ones introduced by Demetriou et al. [39]’s Table 2 and Avrigeanu et al. [42], respectively. As can be seen in both figures, the most consistent level density model potentials and alpha optical model potentials differ from one reaction to another. In both reaction channels, solo employment of the most consistent alpha optical model potentials gave higher cross-section values than the experimental data up to the peak region. After that, calculation results were obtained lower than the experimental data. On the other hand, compared to the case of solo employment of the most compatible alpha optical models, solo employment of the most compatible level density models produced more consistent results with the experimental data. However, the jointly use of the most consistent level density models and the alpha

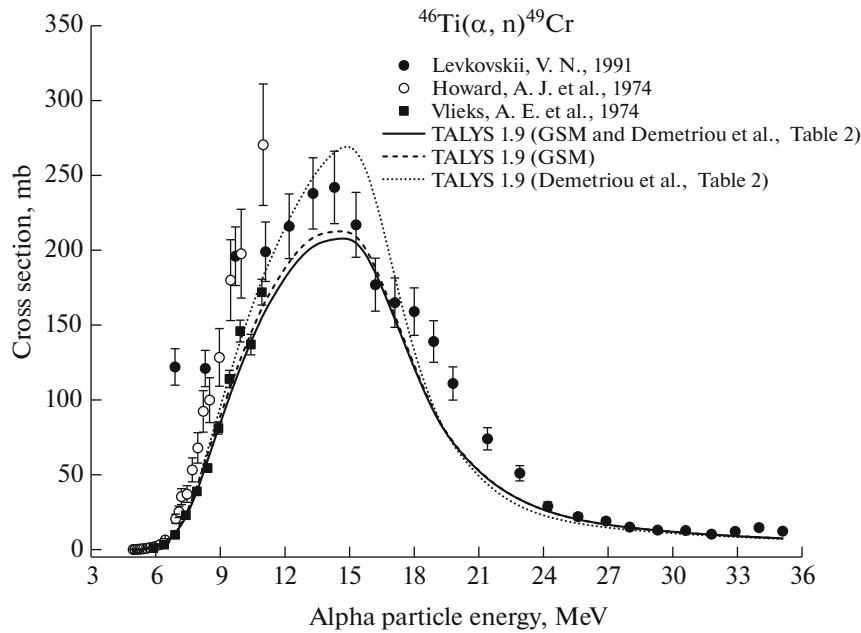


Fig. 1. Cross-section calculation results for the $^{46}\text{Ti}(\alpha, n)^{49}\text{Cr}$ reaction, along with the existing experimental data in the EXFOR library.

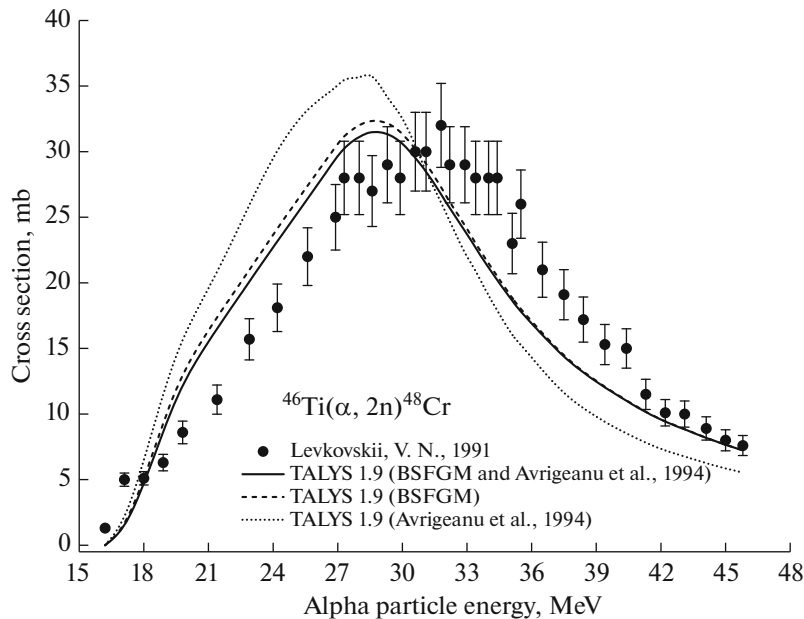


Fig. 2. Cross-section calculation results for the $^{46}\text{Ti}(\alpha, 2n)^{48}\text{Cr}$ reaction, along with the existing experimental data in the EXFOR library.

optical model potentials produced more consistent results with the experimental data than their individual use.

The mean weighted deviation analysis results are presented in Tables 1–4 along with the corresponding results for all the studied reactions.

The results for the $^{50}\text{Cr}(\alpha, n)^{53}\text{Fe}$ and $^{50}\text{Cr}(\alpha, 2n)^{52}\text{Fe}$ reaction channels are presented in Figs. 3

and 4. The energy range of the incident alpha particle for the $^{50}\text{Cr}(\alpha, n)^{53}\text{Fe}$ and the $^{50}\text{Cr}(\alpha, 2n)^{52}\text{Fe}$ reaction channels were taken as 5.4087–10.009 MeV and 14.6–45.8 MeV, respectively, in accordance with the available experimental data. As can be seen in Table 1, the most consistent level density models for these reactions are the GFD and GSM, respectively, while from Tables 2 and 3, it is evident that the most

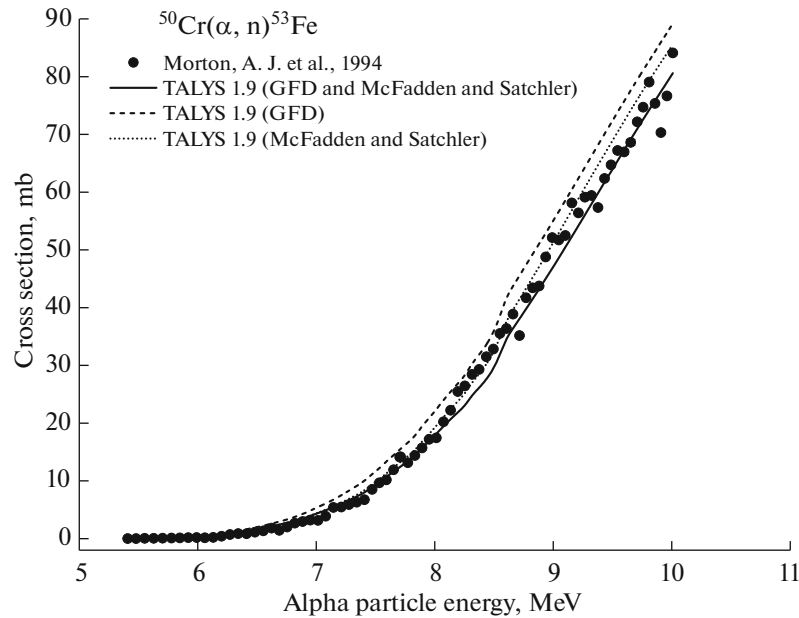


Fig. 3. Cross-section calculation results for the $^{50}\text{Cr}(\alpha, n)^{53}\text{Fe}$ reaction, along with the existing experimental data in the EXFOR library.

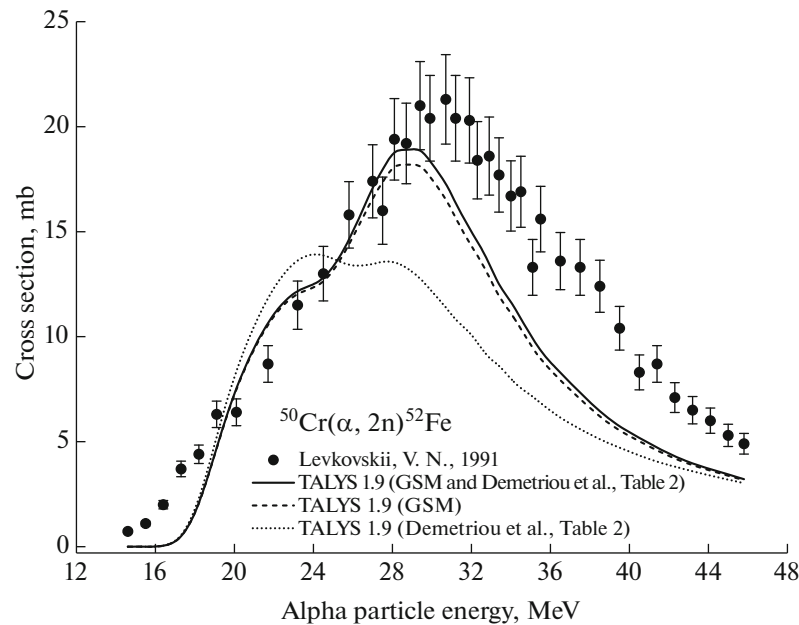


Fig. 4. Cross-section calculation results for the $^{50}\text{Cr}(\alpha, 2n)^{52}\text{Fe}$ reaction, along with the existing experimental data in the EXFOR library.

consistent alpha optical model potentials are the one by McFadden and Satchler for the $^{50}\text{Cr}(\alpha, n)^{53}\text{Fe}$ reaction and the one by Demetriou et al. [39], Table 2 for the $^{50}\text{Cr}(\alpha, 2n)^{52}\text{Fe}$ reaction. For both reaction channels, as it can be seen in Table 4, a significant decrease in the mean weighted deviation analysis is obtained with the combinational use of the models in comparison to their solo employment.

The cross-section theoretical calculations results for the $^{54}\text{Fe}(\alpha, n)^{57}\text{Ni}$ and $^{54}\text{Fe}(\alpha, 2n)^{56}\text{Ni}$ reaction channels are presented in Figs. 5 and 6, respectively, along with the existing experimental data in the EXFOR library. Concerning the $^{54}\text{Fe}(\alpha, n)^{57}\text{Ni}$ reaction, the most consistent level density model is determined to be the GSM and be as BSFGM for the $^{54}\text{Fe}(\alpha, 2n)^{56}\text{Ni}$ reaction. Regarding the alpha optical

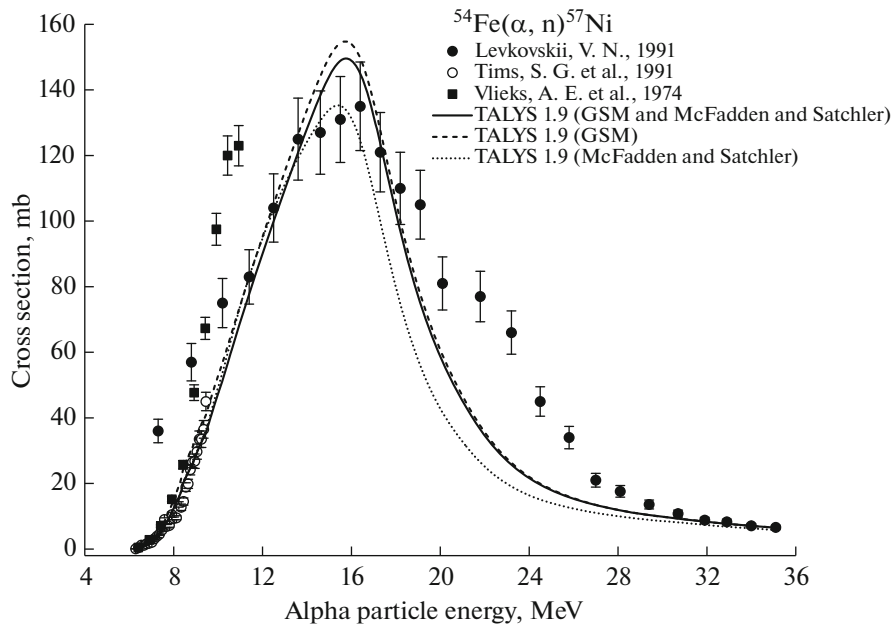


Fig. 5. Cross-section calculation results for the $^{54}\text{Fe}(\alpha, n)^{57}\text{Ni}$ reaction, along with the existing experimental data in the EXFOR library.

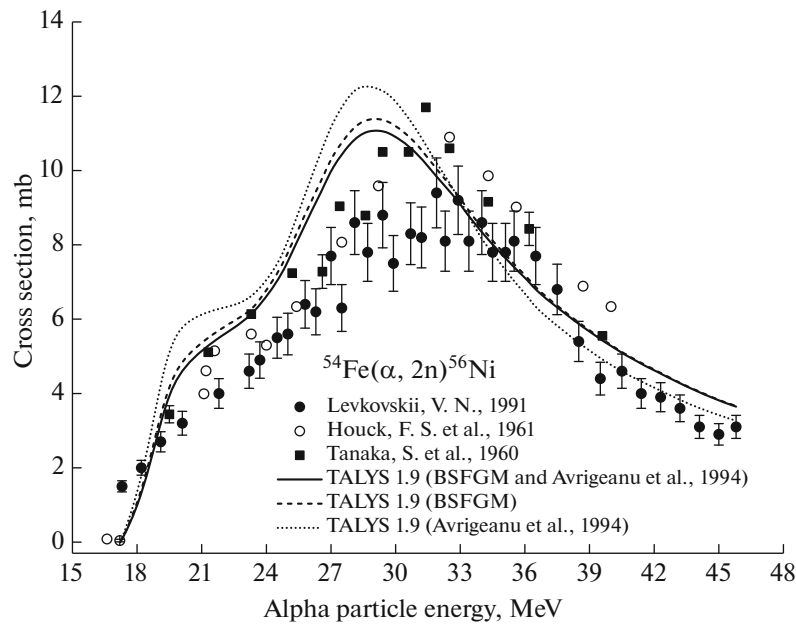


Fig. 6. Cross-section calculation results for the $^{54}\text{Fe}(\alpha, 2n)^{56}\text{Ni}$ reaction, along with the existing experimental data in the EXFOR library.

model potentials, the most consistent results were obtained for the ones introduced by McFadden and Satchler and Avrigeanu et al. [42], respectively. For these reaction channels, it is evident from the graphical representations and the mean weighted deviation analyses that combinational employment of the most consistent level density models and the alpha

optical model potentials generated more consistent outcomes with the experimental data.

The last two reaction channels which were investigated within this study are $^{93}\text{Nb}(\alpha, n)^{96}\text{Tc}$ and $^{93}\text{Nb}(\alpha, 2n)^{95}\text{Tc}$, in which the results are presented in Figs. 7 and 8, respectively. As can be seen in Table 1, the most consistent level density model for the $^{93}\text{Nb}(\alpha, n)^{96}\text{Tc}$ reaction is CT + FGM while it is

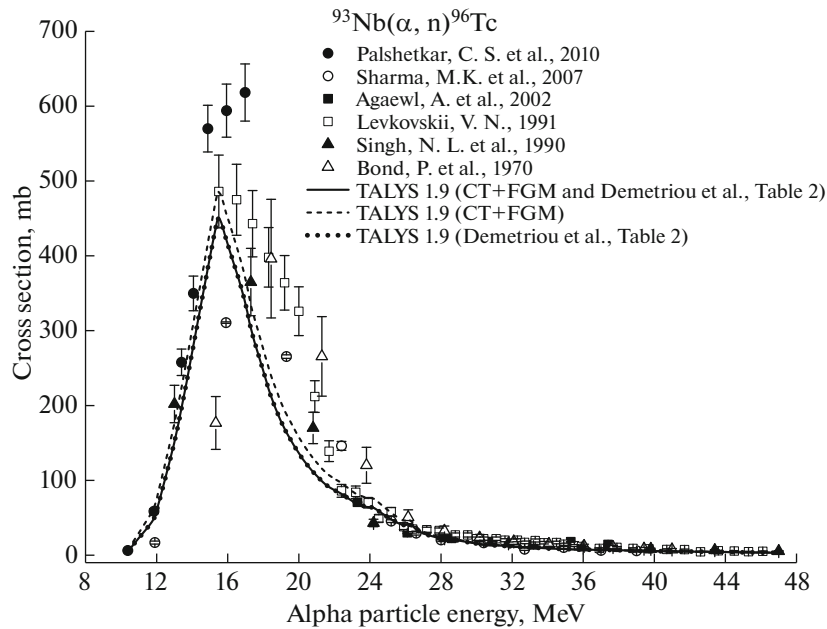


Fig. 7. Cross-section calculation results for the $^{93}\text{Nb}(\alpha, n)^{96}\text{Tc}$ reaction, along with the existing experimental data in the EXFOR library.

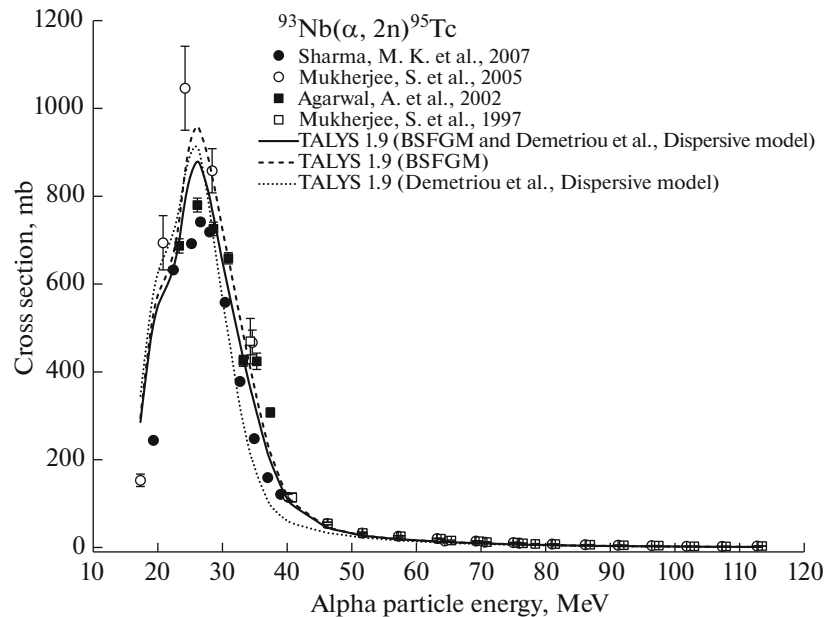


Fig. 8. Cross-section calculation results for the $^{93}\text{Nb}(\alpha, 2n)^{95}\text{Tc}$ reaction, along with the existing experimental data in the EXFOR library.

BSFGM for the $^{93}\text{Nb}(\alpha, 2n)^{95}\text{Tc}$ reaction channel. Regarding the alpha optical model potentials, the most consistent results were obtained for the ones introduced by Demetriou et al. [39], Table 2 and Dispersive Model, respectively, as indicated in Tables 2 and 3. For both reaction channels, Table 4 clarifies the change in the F value which points an enhancement

in the conformity of the theoretical calculations and experimental data.

4. SUMMARY AND CONCLUSION

In this study, cross-section calculations were performed by using the TALYS 1.9 code for the (α, n) and $(\alpha, 2n)$ reactions on fusion materials, such as

Table 2. Mean weighted deviation analysis results of first four alpha optical model potential calculations for each reaction route with respect to the experimental data taken from EXFOR

Reaction Route	TALYS 1.9 Normal Alpha Optical	TALYS 1.9 McFadden and Satchler [38]	TALYS 1.9 Demetriou et al. [39]'s Table 1	TALYS 1.9 Demetriou et al. [39]'s Table 2
$^{46}\text{Ti}(\alpha, n)^{49}\text{Cr}$	3.01629	2.90519	2.94654	2.86926
$^{46}\text{Ti}(\alpha, 2n)^{48}\text{Cr}$	4.73287	4.75873	4.73454	4.75386
$^{50}\text{Cr}(\alpha, n)^{53}\text{Fe}$	55.62269	23.47446	47.39231	42.42444
$^{50}\text{Cr}(\alpha, 2n)^{52}\text{Fe}$	5.23263	5.22669	5.24056	5.21034
$^{54}\text{Fe}(\alpha, n)^{57}\text{Ni}$	4.60326	4.46818	4.50517	4.52466
$^{54}\text{Fe}(\alpha, 2n)^{56}\text{Ni}$	4.49737	4.58488	4.53299	4.56466
$^{93}\text{Nb}(\alpha, n)^{96}\text{Tc}$	14.74112	14.45089	16.18533	13.27485
$^{93}\text{Nb}(\alpha, 2n)^{95}\text{Tc}$	22.77765	22.69428	23.34474	21.41023

Table 3. Mean weighted deviation analysis results of last four alpha optical model potential calculations for each reaction route with respect to the experimental data taken from EXFOR

Reaction Route	TALYS 1.9 Demetriou et al. [39]'s Dispersive Model	TALYS 1.9 Avriganu et al. [40]	TALYS 1.9 Nolte et al. [41]	TALYS 1.9 Avriganu et al. [42]
$^{46}\text{Ti}(\alpha, n)^{49}\text{Cr}$	3.14669	3.19815	11.30725	8.02880
$^{46}\text{Ti}(\alpha, 2n)^{48}\text{Cr}$	4.70541	4.75317	4.69560	4.50611
$^{50}\text{Cr}(\alpha, n)^{53}\text{Fe}$	51.41576	59.21586	236.13660	195.18167
$^{50}\text{Cr}(\alpha, 2n)^{52}\text{Fe}$	5.27269	5.25741	5.25663	5.27548
$^{54}\text{Fe}(\alpha, n)^{57}\text{Ni}$	4.67370	5.06814	15.68170	14.08857
$^{54}\text{Fe}(\alpha, 2n)^{56}\text{Ni}$	4.40399	4.53624	4.36074	4.18550
$^{93}\text{Nb}(\alpha, n)^{96}\text{Tc}$	13.51558	16.56623	31.28912	28.25390
$^{93}\text{Nb}(\alpha, 2n)^{95}\text{Tc}$	21.25665	23.43376	29.11251	26.74542

^{46}Ti , ^{50}Cr , ^{54}Fe and ^{93}Nb . More specifically, all the available level density and optical model parameters were tested and the ones that yielded the most satisfying cross-section results in comparison with the experimental data were presented. Concerning the level density models, the conclusions of this work are the following:

- In the single neutron emitting reaction channels, phenomenological level density model GSM, for the ^{46}Ti and ^{54}Fe target, and CT + FGM, for the ^{93}Nb target, were found to be more appropriate while a microscopic level density model, GFD, generated more consistent outcomes for ^{50}Cr target.

- For the double neutron emitting reaction channels, BSFGM was chosen as the most consistent level density model, except for the $^{50}\text{Cr}(\alpha, 2n)^{52}\text{Fe}$ reaction, for which the GSM was found to be the most suitable.

Regarding the alpha optical model potentials, the conclusions of this work are described below:

- For the single neutron emitting reaction channels, the optical model potential introduced by Demetriou et al. [39]'s Table 2 (see Tables 2 and 3) yielded the most satisfying results for the ^{46}Ti and ^{93}Nb targets, while the one by McFadden and Satchler was the most appropriate for the remaining targets.

Table 4. Mean weighted deviation analysis results of obtained best level density and alpha optical model potential combination calculations for each reaction route with respect to the experimental data taken from EXFOR

Reaction Route	TALYS 1.9 Selected Level Density Model	TALYS 1.9 Selected Alpha Optical Model	TALYS 1.9 Combination of Selected Models
$^{46}\text{Ti}(\alpha, n)^{49}\text{Cr}$	2.89516	2.86926	2.76478
$^{46}\text{Ti}(\alpha, 2n)^{48}\text{Cr}$	3.12142	4.50611	2.98009
$^{50}\text{Cr}(\alpha, n)^{53}\text{Fe}$	44.42287	23.47446	20.83108
$^{50}\text{Cr}(\alpha, 2n)^{52}\text{Fe}$	4.41138	5.21034	4.30469
$^{54}\text{Fe}(\alpha, n)^{57}\text{Ni}$	4.90037	4.46818	4.31664
$^{54}\text{Fe}(\alpha, 2n)^{56}\text{Ni}$	3.44726	4.18550	3.20814
$^{93}\text{Nb}(\alpha, n)^{96}\text{Tc}$	16.56623	13.27485	13.27474
$^{93}\text{Nb}(\alpha, 2n)^{95}\text{Tc}$	21.36944	21.25665	17.30149

- For the double neutron emitting reaction channels, Avrigeanu et al. [42] was chosen as the most consistent alpha optical model potential for the $^{46}\text{Ti}(\alpha, 2n)^{48}\text{Cr}$ and the $^{54}\text{Fe}(\alpha, 2n)^{56}\text{Ni}$ reaction channels. On the other hand, the one by Demetriou et al. [39]'s Dispersive Model and the one by Demetriou et al. [39] Table 2 were the most appropriate alpha optical model potentials for the $^{93}\text{Nb}(\alpha, 2n)^{95}\text{Tc}$ and the $^{50}\text{Cr}(\alpha, 2n)^{52}\text{Fe}$ reaction channels, respectively.

In the all reaction routes examined in this study, the combinational use of the level density models and the alpha optical model potentials generated more consistent results with the experimental data. Thus, the most suitable level density model-alpha optical model potential pairs for the reaction channels examined in this study are introduced to the literature.

The combinational use of the level density models and alpha optical model potentials should be tested for further reactions and more studies should be conducted to provide benefits the theoretical model development studies.

The dependence of the theoretical cross-section calculation results to the level density and alpha optical model potentials are evident and more comprehensive studies should be done to have a better understanding of their effects.

REFERENCES

1. International Energy Agency, World Energy Outlook 2018 (2018).
2. M. Yiğit, J. Fusion Energ. **34**, 1392 (2015).
3. M. Yiğit, Nucl. Sci. Techn. **29**, 55 (2018).
4. A. Aydin, E. Tel, A. Kaplan, and H. Büyükuslu, Ann. Nucl. Energy **37**, 1316 (2010).
5. A. Kaplan, A. Aydin, E. Tel, and H. Büyükuslu, J. Fusion Energ. **29**, 353 (2010).
6. H. Büyükuslu, A. Kaplan, E. Tel, A. Aydin, G. Yıldırım, and M. Bölükdemir, Ann. Nucl. Energy **37**, 534 (2010).
7. A. Kaplan, H. Özdoğan, A. Aydın, and E. Tel, J. Fusion Energ. **32**, 431 (2013).
8. A. Kaplan, M. Şekerci, V. Zapal, and H. Özdoğan, J. Fusion Energ. **36**, 213 (2017).
9. M. Yiğit, Appl. Radiat. Isot. **148**, 108 (2019).
10. H. Özdoğan, Appl. Radiat. Isot. **143**, 1 (2019).
11. H. Özdoğan, M. Şekerci, and A. Kaplan, Mod. Phys. Lett. A **34**, 1950044 (2019).
12. E. Tel, E. G. Aydın, A. Kaplan, and A. Aydin, Indian J. Phys. **83**, 193 (2009).
13. A. Aydin, H. Pekdoğan, E. Tel, and A. Kaplan, Phys. Atom Nucl. **75**, 310 (2012).
14. M. Sahan, E. Tel, H. Sahan, A. Kara, A. Aydin, A. Kaplan, I. H. Sarpun, B. Demir, S. Akca, and E. Yildiz, J. Fusion Energ. **34**, 493 (2015).
15. D. Bucurescu and T. von Egidy, EPJ Web of Conferences **93**, 6003 (2015).
16. A. Nikjou and M. Sadeghi, Appl. Radiat. Isot. **136**, 45 (2018).
17. I. H. Sarpun, A. Aydın, A. Kaplan, H. Koca, and E. Tel, Ann. Nucl. Energy **70**, 175 (2014).
18. A. Aydin, H. Pekdoğan, A. Kaplan, İ. H. Sarpun, E. Tel, and B. Demir, J. Fusion Energ. **34**, 1105 (2015).
19. H. Özdoğan, M. Şekerci, İ. H. Sarpun, and A. Kaplan, Appl. Radiat. Isot. **140**, 29 (2019).
20. M. Sharifian, M. Sadeghi, and M. Alimohamadi, Appl. Radiat. Isot. **151**, 25 (2019).
21. H. Özdoğan, M. Şekerci, and A. Kaplan, Appl. Radiat. Isot. **143**, 6 (2019).

22. İ. H. Sarpün, H. Özdoğan, K. Taşdöven, H. A. Yalim, and A. Kaplan, *Mod. Phys. Lett. A* **34**, 1950210 (2019).
23. J. Lilley, *Nuclear physics: principles and applications*, Wiley (2001).
24. A. Koning, S. Hilaire, and S. Goriely, TALYS-1.9 A nuclear reaction program, User Manual (2017), URL https://tendl.web.psi.ch/tendl_2019/talys.html.
25. V. V. Zerkin and B. Pritychenko, *Nucl. Instrum. Methods Phys. Res. A* **888**, 31 (2018).
26. N. Kurenkov, V. Lunev, and Y. Shubin, *Appl. Radiat. Isot.* **50**, 541 (1999).
27. A. Gilbert and A. G. W. Cameron, *Can. J. Phys.* **43**, 1446 (1965).
28. A. V. Ignatyuk, K. K. Istekov, and G. N. Smirenkin, *Yad. Fiz.* **29**, 875 (1979).
29. H. Baba, *Nucl. Phys. A* **159**, 625 (1970).
30. W. Dilg, W. Schantl, H. Vonach, and M. Uhl, *Nucl. Phys. A* **217**, 269 (1973).
31. A. V. Ignatyuk, G. N. Smirenkin, and A. S. Tishin, *Yad. Fiz.* **21**, 485 (1975).
32. A. Koning, S. Hilaire, and S. Goriely, *Nuclear Physics A* **810**, 13 (2017).
33. S. Goriely, S. Hilaire, and A. J. Koning, *Phys. Rev. C* **78**, 064307 (2008).
34. S. Hilaire and S. Goriely, *Nucl. Phys. A* **779**, 63 (2006).
35. S. Hilaire, M. Girod, S. Goriely, and A. J. Koning, *Phys. Rev. C* **86**, 064317 (2012).
36. E. Fermi, *Z. Phys.* **36**, 902 (1926).
37. A. Koning and J. Delaroche, *Nucl. Phys. A* **713**, 231 (2003).
38. L. McFadden and G. R. Satchler, *Nucl. Phys.* **84**, 177 (1966).
39. P. Demetriou, C. Grama, and S. Goriely, *Nucl. Phys. A* **707**, 253 (2002).
40. V. Avrigeanu, M. Avrigeanu, and C. Manaiescu, *Phys. Rev. C* **90**, 044612 (2014).
41. M. Nolte, H. Machner, and J. Bojowald, *Phys. Rev. C* **36**, 1312 (1987).
42. V. Avrigeanu, P. E. Hodgson, and M. Avrigeanu, *Phys. Rev. C* **49**, 2136 (1994).